Popular Summary

Validation and Determination of Ice Water Content – Radar Reflectivity Relationships during CRYSTAL-FACE: Flight Requirements for Future

D. S. Sayres[1], J.B. Smith[1], J.V. Pittman[1,5], E.M. Weinstock[1], J.G. Anderson[1], G. Heymsfield[2], L. Li[3], A.M. Fridland[4], A.S. Ackerman[4]

[1]Department of Earth and Planetary Sciences, Harvard University
[2]Goddard Space Flight Center
[3]UMBC/GEST
[4]NASA Goddard Institute for Space Studies
[5]Marshall Space Flight Center

In order for clouds to be more accurately represented in global circulation models (GCM), there is need for improved understanding of the properties of ice such as the total water in ice clouds, called ice water content (IWC), ice particle sizes and their shapes. Improved representation of clouds in models will enable GCMs to better predict for example, how changes in emissions of pollutants affect cloud formation and evolution, upper tropospheric water vapor, and the radiative budget of the atmosphere that is crucial for climate change studies. An extensive cloud measurement campaign called CRYSTAL-FACE was conducted during Summer 2002 using instrumented aircraft and a variety of instruments to measure properties of ice clouds. This paper deals with the measurement of IWC using the Harvard water vapor and total water instruments on the NASA WB-57 high-altitude aircraft. The IWC is measured directly by these instruments at the altitude of the WB-57, and it is compared with remote measurements from the Goddard Cloud Radar System (CRS) on the NASA ER-2. CRS measures vertical profiles of radar reflectivity from which IWC can be estimated at the WB-57 altitude. The IWC measurements obtained from the Harvard instruments and CRS were found to be within 20-30% of each other. Part of this difference was attributed to errors associated with comparing two measurements that are not collocated in time an space since both aircraft were not in identical locations. This study provides some credibility to the Harvard and CRS-derived IWC measurements that are in general difficult to validate except through consistency checks using different measurement approaches.

Validation and determination of ice water content - radar reflectivity relationships during CRYSTAL-FACE: Flight requirements for future comparisons

D. S. Sayres,[1] J. B. Smith,[1] J. V. Pittman,[1,5] E. M. Weinstock,[1] J. G. Anderson,[1] G. Heymsfield,[2] L. Li[3] A. M. Fridlind[4] A. S. Ackerman[4]

D. S. Sayres, Department of Earth and Planetary Sciences, Anderson Group/CCB, Harvard University, 12 Oxford Street, Link 261, Cambridge, MA 02138. (sayres@huarp.harvard.edu)

[1]Department of Earth and Planetary Sciences, Harvard University, Cambridge, MA 02138

[2]Goddard Space Flight Center, NASA, Greenbelt, MD 20771

[3]University of Maryland, Baltimore County, Baltimore, MD 21250

[4]NASA Goddard Institute for Space Studies, New York, NY 10025

[5]Marshall Space Flight Center, NASA, Huntsville, AL 35805

Abstract.   In situ measurements of cirrus ice water content (IWC) by the

Harvard waper vapor and total water instruments onboard the NASA WB-

57 during CRYSTAL-FACE are compared with remote sensing data made

by the Cloud Radar System (CRS) instrument from the NASA ER-2. The

comparisons are used to show that for measurements of in situ IWC and re-

motely measured radar reflectivity (Z_e) collocated within 2 kilometers of each

other, a single IWC-Z_e relationship can be found that fits the data with an

uncertainty of $\pm$20-30%. A cloud resolving model shows this level of uncer-

tainty to be consistent with sampling errors associated with comparing two

measurements that are not collocated. Satellite-borne remote sensing mea-

surements from CloudSAT and CALIPSO will soon provide the vertical struc-

ture of clouds on a global scale. Uncertainties are quantified in the use of in

situ data to validate the retrieval algorithms used to derive the IWC of clouds

from remote sensing observations, such as radar reflectivity (Z_e). Uncertain-

ties are classified into instrumental uncertainties, uncertainties related to sam-

pling errors, and uncertainties in using a single IWC-Z_e relationship to de-

scribe a cloud.

1. Introduction

Clouds play a critical role in determining the radiative budget of the atmosphere and surface by the absorption and scattering of solar and terrestrial radiation [*Norris*, 2000]. The extent to which clouds scatter and absorb radiation is determined by the microphysical and geometric structure of the cloud [*Baran*, 2005]. In order for clouds to be represented more accurately in GCMs the vertical structure of ice water content (IWC), particle size distribution, and particle geometry (habit) in clouds needs to be obtained on a global scale [*Stephens et al.*, 2002]. Accurately representing clouds in general circulation models (GCMs) and climate models is paramount for enabling models to predict how changes in emissions of pollutants will affect cloud formation and evolution, upper tropospheric water vapor, and the radiative budget of the atmosphere. However, to date cloud processes represent one of the largest uncertainties in GCMs [*Stephens*, 2005].

In order to improve our understanding of cloud physics several measurement campaigns using balloon and aircraft *in situ* measurements have been devoted to studying the micro and macrophysical properties of clouds [*Pawlowska et al.*, 2000; *Gultepe et al.*, 2001; *Buschmann et al.*, 2002; *Nasiri et al.*, 2002, and references therein]. While *in situ* measurements provide high spatial resolution, they typically provide only a one dimensional trajectory through a cloud and within the limit of aircraft flight time can only sample a small fraction of a cloud. In recent years remote sensing probes such as radar and lidar have become central to the effort to quantitatively measure microphysical properties of clouds on a large scale. The culmination of this effort is NASA's launch of a suite of satellites known as the A-Train [*Stephens et al.*, 2002]. The A-Train consists of six satellites

flying in formation so that all make observations of the same volume of atmosphere within 15 minutes of each other. CloudSat, a 94 GHz cloud profiling radar, and CALIPSO, a two channel (532 and 1064 nm) cloud and aerosol lidar, are focused on making high resolution measurements of the microphysical properties of clouds such as IWC, median ice particle volume diameter, and particle shape.

The physical properties of clouds are deduced by remote sensing instruments from the attenuation and scattering of radar and lidar signals or by their infrared emission. Radar instruments measure the reflectivity from cloud particles caused by the angular dependence of scattering of the radar beam. The reflectivity, Z_e, can be related related to the IWC of the cloud via a power-law relationship detailed in section 2. Since different clouds, and regions within a cloud, possess different particle-size distributions, habits, and ice densities, a suite of relationships, each set representing a particular category of cloud, is required to describe an ensemble of cloud types. To determine which relationship to use for a particular cloud and to minimize the uncertainty in the IWC-Z_e relationships, several approaches have been suggested using the extinction coefficient from lidar [*Wang and Sassen*, 2002a, b], the mean Doppler velocity [*Donovan*, 2003], or cloud top temperature [*Liu and Illingworth*, 2000]. However, given the ability to categorize clouds based on remote measurements, great importance still must be placed on obtaining and validating coefficients for each cloud type.

The first step in deriving IWC-Z_e relationships for different clouds is to obtain IWC and the corresponding Z_e. Previous comparisons have used *in situ* particle size data [*Brown and Illingworth*, 1995; *Liu and Illingworth*, 2000] or modeled size spectra of pure hexagonal columns and plates to derive IWC and Z_e [*Aydin and Tang*, 1997; *Sassen et al.*,

2002]. These studies have reported uncertainties in the derived IWC of as much as 60% for a given value of Z_e. For the comparison presented here we use direct measurements of *in situ* IWC and remotely detected radar reflectivity obtained during the Cirrus Regional Study of Tropical Anvils and Cirrus Layers - Florida Area Cirrus Experiment (CRYSTAL-FACE) [*Jensen et al.*, 2004].

The interpretation of this comparison is complicated by the spatial and temporal differences between the air parcels that the *in situ* and remote instruments measure. To address the uncertainties inherent in comparing IWC from *in situ* and remote measurements we group the uncertainties into three categories, not only to best constrain the parameters that are needed to derive IWC from Z_e, but also to try to determine the most efficient way to carry out these validation experiments.

1. Instrumental uncertainties in the measurement of IWC and radar reflectivity. These uncertainties are assumed to be fixed for a given comparison and independent of the cloud being measured.

2. Uncertainty in matching *in situ* data with remote data, which we refer to as sampling error. This error occurs due to the reality that there is often spatial or temporal separation between the *in situ* measurement and the remote measurement. Due to the large variability of IWC, or cloud inhomogeneities, measurements that are not collocated can lead to erroneous (non-instrumental) errors in the comparison.

3. Uncertainty in the relationships used to calculate IWC from Z_e. This uncertainty includes the sensitivity of the constants used in this calculation to variations in habit, size distribution, and ice density. This category also includes estimates of the uncertainty resulting from cloud type variability.

89   Instrumental uncertainties and the error in derived IWC are discussed in Section 3.1.

90   Section 3.2 discusses the comparisons made during the CRYSTAL-FACE mission and the

91   uncertainty associated with using different IWC-Z_e relationships. Section 4 uses a cloud

92   model to evaluate the error associated with insufficient overlap between two instrument

93   measurements.

2. Physical basis for the IWC-Z_e relationship

94   The magnitude of the radar reflectivity, Z, due to Rayleigh scattering is proportional

95   to $\int n(D)D^6\, dD$, where n is the number density of particles with diameter, D [*Liao and*

96   *Sassen*, 1994]. However, this is only valid for small spheroidal particles and does not

97   account for Mie scattering or the effect of particle shape and density. Equation 1 is a

98   modified form of this relationship proposed by *Liu and Illingworth* [2000], where a term

99   accounting for particle shape has been added.

$$Z = \int n(D)D^6 K(m,\rho)^2 f(D,\rho)h(D,\rho)/0.93\, dD, \tag{1}$$

101   where K is a factor dependent on the refractive index of ice, m, f is the ratio of Mie to

102   Rayleigh scattering, h is a shape factor dependent upon the habit of the particles, and

103   the factor 0.93 is chosen so that for liquid water the relationship reduces to the equation

104   for spheroidal droplets.

105   IWC, defined as the mass of ice per unit volume of air, can be written as

$$IWC = \int \rho V n(D)\, dD, \tag{2}$$

107   where n is the number density of particles with volume, V, and mass density, ρ. By

108   inspection of Equations 1 and 2, Z is proportional to the square of IWC. The relationship

109   between IWC and Z_e, the equivalent reflectivity for ice, can thus be written as a power

law,

$$IWC = aZ_e^b, \tag{3}$$

where IWC is measured in g/m^3, Z_e is measured in $mm^6 m^{-3}$, and a and b are functions of particle size distribution, habit, and ice density. Given measurements of IWC and corresponding Z_e values, the coefficients a and b are determined empirically by regression of IWC with Z_e.

3. Direct comparisons of *in situ* IWC and remote Z_e data

The CRYSTAL-FACE campaign took place out of Key West, Florida during July, 2002. The main focus of the mission was to study the physical properties of subtropical cirrus clouds in order to improve our understanding of the formation and evolution of cirrus and to improve our ability to model cirrus in GCMs. In order to accomplish this objective, several aircraft were used, each carrying a different suite of instruments and each measuring a different level of the atmosphere. Another goal of CRYSTAL-FACE was to compare and validate remote sensing instruments flown on the ER-2 with *in situ* measurements from the WB-57. The ER-2 carried remote sensing instruments similar to those that are part of the A-Train constellation of satellites. The Cloud Radar System (CRS) and Cloud Physics Lidar (CPL) have similar capabilities to the instruments aboard the CloudSat and CALIPSO Satellites, respectively. The WB-57 carried a suite of *in situ* instruments measuring IWC (Harvard Total Water and Water Vapor), particle size distributions, habit, and aerosols, as well as tracer and meteorological measurements.

3.1. Flight Plans and Instruments

129   As an example of coordinated flight segments used to compare remote and in situ

130   IWC measurements, we show in figure 1 the flight track of the WB-57 (left image) and

131   ER-2 (right image) during the flight of July 16th. The ER-2 made several passes over

132   a convective system that developed over Florida and moved westward, while the WB-57

133   made several passes through the cirrus outflow of the same convective system. This makes

134   the flight of July 16th ideal for comparing remote and *in situ* data. While during other

135   flights the ER-2 and WB-57 flew together, they were sampling several different clouds and

136   therefore did not sample air parcels close enough in time and space to make reasonable

137   comparisons. For the purpose of this comparison we focus on IWC retrieved from radar

138   and measured *in situ*. Radar reflectivity was measured using the Cloud Radar System

139   (CRS) instrument that flew aboard the ER-2 aircraft and IWC was measured using the

140   Harvard Lyman-α total water (HV-TW) and water vapor hygrometers aboard the WB-57.

141   The CRS instrument is a 94 GHz Doppler, polarimetric radar mounted in the right

142   wing pod of the ER-2 [*Li et al.*, 2004]. The 94 GHz frequency allows CRS to measure a

143   wide range of clouds, from thin cirrus to thick convective anvils. The units of reflectivity

144   (Z_e) are $mm^6 m^{-3}$. However, Z_e is often reported in units of power (dB) where $1\,dB =$

145   $10 log_{10}(mm^6 m^{-3})$. The sensitivity of the CRS instrument is -29 dB ($3.65 \times 10^{-3} g/m^3$

146   of condensate) allowing it to detect 99% of radiatively significant clouds at midlatitudes

147   and 92% in the tropics [*Brown and Illingworth*, 1995]. Radiatively significant clouds are

148   defined as those that cause differences from clear sky values of more than 10 Wm^{-2} in

149   outgoing longwave radiation or in the longwave flux divergence within a cloud layer and 5

150   Wm^{-2} in the downward longwave flux. To maintain the calibration of the radar, average

151   transmit power and receiver gain are continuously monitored in order to have in-flight

152 diagnostics as to the transmitter stability. In addition, external calibration against other

153 radar systems yields an uncertainty of 1 dB, which is equivalent to a 15% uncertainty in

154 the retrieved IWC. The spatial resolution of the reflectivity data reported by the CRS

155 instrument for the CRYSTAL-FACE mission is 1 km horizontally and 75 meters vertically

156 along the flight path of the ER-2 . A retrieval algorithm using the *Brown and Illingworth*

157 [1995] relationship was used to calculate the archived remote IWC data. The coefficients

158 used for the retrieval are derived from ice crystal size spectra from a 2D optical array

159 probe sampling cirrus from midlatitude frontal systems. The size spectra are converted

160 to IWC and radar reflectivities via equations similar to Equations 2 and 1, respectively.

161 For the IWC the bulk density is assumed to be proportional to $D^{-1.1}$, where D is the

162 mean volume diameter of the particles. A simple least squares fit to Equation 3 yields

163 the parameters a and b. The CRS data use a K^2 value of 0.695 which is appropriate

164 at 94 GHz under 0°C conditions. However, previous measurements have used K^2 equal

165 to 0.93 in order that the reflectivities be scaled to liquid water. In order to compare

166 the data presented here with previous measurements, we have rescaled the CRS data by

167 subtracting 1.26 dB.

168 HV-TW measures total water (i.e. vapor + ice) directly. IWC is derived by subtracting

169 water vapor, as measured by the Harvard water vapor instrument, from total water.

170 Both Harvard water vapor and total water measure water vapor by using Lyman-α to

171 photodissociate water into an OH fragment in its first excited electronic state. The excited

172 OH fragment then either relaxes via fluorescence or is quenched during a collision with an

173 air molecule. Within the range of ambient densities encountered during CRYSTAL-FACE,

the magnitude of the fluorescence signal is directly proportional to the mixing ratio of water.

Calibrations are performed at a range of pressures and water vapor mixing ratios [*Weinstock et al.*, 2006a]. Water vapor is injected into the calibration system using a bubbler and checked via longpath and shortpath (axial) absorption. The calibration is therefore tied to two fundamental standards: the vapor pressure of water over liquid at room temperature and the absorption cross section of water vapor at the Lyman-α wavelength. In-flight validation consists of cross checking changes in the ambient water vaper mixing ratio (i.e. ΔH_2O) using both dual-path (axial) absorption and fluorescence. In addition, in clear air, the Total Water instrument is compared to the Water Vapor instrument. Agreement between the two instruments increases confidence in the water vapor measurement and the IWC product [*Weinstock et al.*, 2006b].

During flight operation, the HV-TW instrument uses a roots pump downstream of the detection axis to pull ice particles and water vapor into the instrument duct while maintaining isokinetic flow to ensure that the number density of particles entering the inlet is the same as the ambient number density. A 600-Watt inlet heater evaporates the ice particles and the total water is measured. The precision of the total water instrument is 5% and the accuracy with respect to ice water content is 15% [*Weinstock et al.*, 2006a]. The HV-TW uses a 1 second integration time and due to the speed of the aircraft this yields a horizontal resolution of 100-200 meters. For the purposes of this comparison, 10 second data, which produces 1.5 km averages, are used in order to make the horizontal resolution consistent with that of the CRS instrument.

3.2. Direct Comparison of Data

196 If both the ER-2 and WB-57 were coordinated so that the instruments were always

197 sampling the same footprint at the same time, then a direct comparison between the in-

198 struments would be straightforward. However, because of constraints on aircraft velocities

199 and air traffic control, most of the time the instruments will not be sampling the same

200 air parcel. Instead there will be some finite distance and time between when the cloud

201 is sampled by the *in situ* instrument and the cloud is sampled by the remote sensing in-

202 strument. It is therefore imperative that these spatial and temporal differences be taken

203 into account and ideally minimized when making the comparison. We first address the

204 temporal difference between when the ER-2 and WB-57 sample a region by making a first

205 order correction for the movement of air parcels using the wind velocity measured aboard

206 the WB-57 by the Meteorological Measurement System (MMS). A detailed description of

207 the derivation of wind velocity from MMS measurements is given by *Scott et al.* [1990].

208 For the cloud encounter shown in Figure 1, the ER-2 took approximately 10 minutes to

209 traverse the cloud and the WB-57 lagged the ER-2 by between 2 and 8 minutes. For each

210 time interval that data are reported along the ER-2 flight track, the air parcels sampled

211 by the WB-57 are advected back to where they would have been at the time the CRS

212 instrument made a measurement. The air parcel sampled by the HV-TW instrument that

213 is nearest to the air parcel sampled by the CRS instrument is then used in the comparison.

214 The result for a cloud sampled during the flight on July 16th is shown in Figure 2, where

215 the black and green points represent the flight tracks of the ER-2 and WB-57, respectively,

216 and the blue triangles correspond to the air parcels sampled by the WB-57 advected by

217 the winds measured along the WB-57 flight track during the time lag between the ER-2

218 and WB-57 cloud encounter. As is evident in the figure, even within a few minutes there

219 can be considerable movement of air parcels.

220   Figure 3 shows the *in situ* HV-TW and retrieved CRS IWC plotted versus time along

221 the ER-2 flight track in blue and green, respectively. The left-hand plot shows data taken

222 during a flight transect through a cloud on July 16th between 79600 and 80200 seconds

223 UT. The colored points on the bottom of the plot show the horizontal distance between

224 the air parcels sampled by HV-TW and CRS with dark blue being points separated by

225 a few hundred meters and red being points separated by more than 3 kilometers. The

226 horizontal separation distance is the distance after the air parcels sampled by HV-TW

227 have been advected as described earlier. For the data shown in the left plot of Figure 3,

228 the distance between the air parcels being sampled ranges from a few hundred meters to

229 two kilometers. For this comparison the retrieved IWC agrees with the *in situ* IWC to

230 within 20% and, in general, reproduces the structure of IWC in the cloud.

231   If we now look at a case where the sampled air parcels are five kilometers away from

232 each other (right plot of Figure 3), the two measurements do not agree because, while

233 the strength and direction of the wind have been accounted for, the IWC in a cloud

234 varies significantly in magnitude and structure even over a few kilometers. This is ev-

235 ident in several other examples where the measurements agree fairly well when the air

236 parcels being sampled are within two kilometers and the comparison breaks down as the

237 distance between the parcels becomes greater than 2 kilometers. This is consistent with

238 the modeled sampling error caused by inadequate spatial overlap discussed in section 4.

239 The maximum acceptable distance for a reasonable comparison will depend on the level

240 of cloud inhomogeneities, with 2 kilometers being the distance associated with the clouds

241 sampled during CRYSTAL-FACE. By limiting the comparison to flight legs where both

242 the ER-2 and WB-57 were within 2 kilometers of each other, the error caused by insuffi-

243 cient spatial overlap should be small at least for clouds with comparable inhomogeneities.

244 During the month long CRYSTAL-FACE mission there were only 8 flight legs where both

245 aircraft sampled clouds within 2 kilometers of each other. This results in only 37 minutes

246 of data out of approximately 70 hours of flight time.

247   The comparisons shown in Figure 3 use IWC derived from Z_e using the *Brown and*

248 *Illingworth* [1995] relationship. However, the parameters in this relationship were derived

249 from tropical cirrus clouds and are possibly not appropriate for the anvil cirrus sampled

250 during CRYSTAL-FACE. In order to determine which IWC-Z_e relationship best fits the

251 CRYSTAL-FACE data, a linear least squares fit to Equation 4 is performed to derive the

252 coefficients a and b for each flight leg where data from HV-TW and CRS are within 2

253 kilometers. We convert Equation 3 from $mm^6 m^{-3}$ because CRS reports Z_e in terms of

254 dB. This results in the linear equation,

$$log_{10}(IWC) = log_{10}(a) + \frac{b}{10} * Z_e \qquad (4)$$

256 The data are fit by minimizing the weighted residuals in both variables. The data are

257 weighted using a 1 dB uncertainty in radar reflectivity and a 15% uncertainty in IWC.

258 Shown in Figure 4 are regressions of $log_{10}(IWC)$ versus Z_e for data that are within 2

259 kilometers of each other along with the least squares fits to the data. In Figure 4a each

260 of the flight legs is plotted in a different color as indicated by the figure legend. Also

261 shown are the least square fits to each data set. There is considerable variation in the

262 slope of the best fit line between the data sets. However, a single best fit line can be

263 found that fits all the data to within ±20%. The least squares fit to all the data is shown

264 in Figure 4b as a dark-gray thick dashed line. Also shown are the IWC-Z_e relationships

265 using the coefficients from Liu [2000], Brown [1995], and Aydin [1997] as dashed lines in

266 the three lighter shades of gray. The coefficients derived from this work as well as those

267 from previous comparisons are listed in Table 1. The Table also includes characterizations

268 of the clouds used in each study.

269   Figure 5 shows the eight comparisons that were made during CRYSTAL-FACE. The

270 comparisons are divided by cloud thickness, with thin cirrus plotted in the top four plots

271 and thick cirrus plotted in the bottom four plots. For each comparison plot, the *in situ*

272 IWC data from the HV-TW instrument are plotted in black and the derived IWC data

273 using the fit coefficients from this work are plotted in blue. Also shown are derived IWC

274 data using the relationships described in Brown [1995], Liu [2000], Sassen [1987], and

275 Aydin [1997] in purple, magenta, cyan, and red, respectively. For three of the four thin

276 cirrus cases (Figure 5, plots *a*, *c*, and *d*), the coefficients from this work, as well as those

277 listed in Table 1 agree well with the *in situ* IWC data. In contrast, for the comparison

278 from July 11th (Figure 5, plot *b*), all the relationships underpredict the amount of ice

279 by between 25 and 50%. However, this can possibly be attributed to the predominance

280 of small particles as this is the thinnest cirrus layer presented in this comparison. For

281 the thick cirrus cases, all of which are from July 16th, the agreement between *in situ*

282 and remote data vary between a few percent and 60% depending on which relationship

283 is used. For the comparisons shown in plots *e* and *f*, the Brown [1995], Liu [2000] and

284 coefficients from this work agree with the *in situ* IWC to within 20%. For the comparison

285 shown in plot *g*, the Aydin [1997] and Sassen [1987] give the best agreement, and for the

286 comparison shown in plot *h* none of the parametrizations agree well over the whole flight

287 leg, with differences ranging from 10 to 30%. However, this is also the case with the worst

288 spatial overlap with distances ranging between 1 and 2.5 km. The comparisons presented

289 in Figures 4 and 5 show that a single IWC-Z_e relationship is able to reproduce the IWC

290 from *in situ* data to within a few percent to 30% depending on the flight leg. The question

291 that now must be addressed is whether this variability in agreement represents variability

292 in the IWC-Z_e relationship or is due to sampling error.

4. Quantifying sampling error due to inadequate spatial overlap

293   In order to quantify the sampling errors associated with comparing measurements that

294 are not collocated, synthetic clouds, of the type observed during CRYSTAL-FACE, are

295 generated using DHARMA, a cloud resolving microphysics model [*Ackerman et al.*, 2004;

296 *Fridlind et al.*, 2004; *Stevens et al.*, 2002]. The output from the model simulates the

297 cirrus cloud inhomogeneities observed during CRYSTAL-FACE making it well suited for

298 studying the sampling error between measurements that are not collocated. The results

299 presented here use simulations of the clouds sampled by the WB-57 and ER-2 on July

300 16th and 18th. We use a simulation to evaluate sampling error in order to temporarily

301 remove the uncertainties associated with the instruments or with deriving IWC from Z_e

302 from the analysis. This means that any differences between two synthetic measurements

303 from the simulation must be caused by sampling error resulting from insufficient overlap

304 between the two measurements.

305   To quantify how close two measurements must be to each other in order to ensure that

306 the sampling error is less than or comparable to the instrument uncertainty we calculate

307 the average error between measurements of IWC by two aircraft flying parallel to each

308 other, but separated by some distance. By using different transects through the simulated

cloud at different altitudes, the sampling error can be calculated for different spatial

separations and different levels of cloud inhomogeneity. In Figure 6, IWC is plotted at a

particular altitude within a cloud, in this case a simulation of the could system sampled

by the WB-57 and ER-2 on July 16th, 2002. The upper contour plot is a horizontal slice

through the cloud at an altitude of 16.3 km and the lower contour plot is at an altitude

of 15.6 km. Both plots show contours of IWC in g/m^3 as indicated by the color bar to

the right of each plot. The graphs below each contour plot show the fractional difference

between two measurements separated by a distance of 0 to 10 km for each altitude, with

the median value for each separation distance plotted as squares. For the horizontal slice

at 16.3 km, the error caused by two aircraft sampling parcels that are separated by 1

km is 15% and by 2 km is 30%. For the horizontal slice at 15.6 km, the error caused by

two aircraft sampling parcels that are separated by 1 km is 10% and by 2 km is 20%. It

is important to note that the level of inhomogeneities in the cloud have a large vertical

dependence, and therefore the restrictions on the coordination of two aircraft may depend

both on the type of cloud and location within a particular cloud. To reduce the necessity

of coordinating two aircraft to be collocated horizontally to within 1 to 2 km, the *in situ*

aircraft would ideally be sampling in the thicker parts of the cirrus.

5. Conclusions

The comparisons between *in situ* IWC and remotely measured Z_e made during the

CRYSTAL-FACE mission show a consistent IWC-Z_e relationship for the cirrus clouds

sampled over Florida, within the uncertainty due to sampling error. This was the first

comparison in which both *in situ* IWC and remote measured Z_e were used, as previous

studies relied on converting particle size spectra into IWC and Z_e. The agreement observed

331 between *in situ* IWC and IWC derived from Z_e is approximately 20% when comparing

332 *in situ* air parcels that were within 2 km of remotely measured air parcels. Previous

333 comparisons based on particle size distributions found errors of +50% to -30% in IWC for

334 a given Z_e [*Liu and Illingworth*, 2000]. Due to the requirement that the air parcels sampled

335 by *in situ* and remote instruments be collocated to within 2 km, during the CRYSTAL-

336 FACE mission only 37 minutes out of more than 70 hours of flight time are usable for direct

337 comparisons. This restriction on which comparisons can be used is important since once

338 the sampling error becomes larger than the instrument uncertainty, it is not possible to

339 distinguish variability in the IWC-Z_e relationship due to microphysical differences between

340 the cloud samples from sampling error. Most of the flight legs presented in this work were

341 made on July 16th, which means that the relationship derived has only been validated for

342 a single cloud. In order to both derive IWC-Z_e relationships for different types of clouds

343 and to validate IWC retrieval algorithms for either airborne- or satellite- based radar, the

344 frequency of valid comparison oppurtunities for a flight mission must be increased.

345 To quantify the uncertainty associated with sampling error, we have used the DHARMA

346 model to simulate the cirrus sampled during CRYSTAL-FACE. The model predicts that

347 a sampling error of 20 to 30% for air parcels separated by 2 km would be expected

348 for the cirrus encountered during CRYSTAL-FACE. This means that the discrepancies

349 between *in situ* IWC and IWC derived from Z_e during CRYSTAL-FACE are consistent

350 with the expected sampling error due to the measurements not being collocated, and

351 do not indicate that several IWC-Z_e relationships are necessary to explain the clouds

352 sampled during CRYSTAL-FACE. The maximum allowable separation distance will vary

353 for different clouds, since the sampling error depends on cloud inhomogeneities.

354 While the results from the CRYSTAL-FACE mission seem promising, a much larger data

355 set is needed in order to evaluate how well a single IWC-Z_e relationship describes similar

356 types of clouds. Given the importance of clouds in the climate system and the importance

357 of having quantitative measurements from A-Train satellites, aircraft campaigns will have

358 to be able to provide large quantities of *in situ* data with sufficient overlap in order to

359 quantitatively validate remote sensing instruments.

References

365 Ackerman, A. S., M. P. Kirkpatrick, D. E. Stevens, and O. B. Toon (2004), The impact

366   of humidity above stratiform clouds on indirect aerosol climate forcing, *Nature, 432,*

367   1014–1017.

368 Atlas, D., S. Y. Matrosov, A. J. Heymsfield, M.-D. Chou, and D. B. Wolf (1995), Radar

369   and radiation properties of ice clouds, *Journal of Applied Meteorology, 34,* 2329–2345.

370 Aydin, K., and C. X. Tang (1997), Relationships between iwc and polarimetric radar mea-

371   surands at 94 and 220 ghz for hexagonal columns and plates, *Journal Of Atmospheric

372   And Oceanic Technology, 14,* 1055–1063.

373 Baran, A. J. (2005), The dependence of cirrus infrared radiative properties on ice crystal

374   geometry and shape of the size-distribution function, *Quarterly Journal of the Royal*

375 *Meteorological Society, 131*(607), 1129–1142.

376 Brown, P. R. A., and A. J. Illingworth (1995), The role of spaceborne millimeter-wave

377 radar in the global monitoring of ice cloud, *Journal of Applied Meteorology, 34*, 2346–

378 2366.

379 Buschmann, N., G. M. McFarquhar, and A. J. Heymsfield (2002), Effects of observed

380 horizontal inhomogeneities within cirrus clouds on solar radiative transfer, *Journal Of*

381 *Geophysical Research-Atmospheres, 107*.

382 Donovan, D. P. (2003), Ice-cloud effective particle size parameterization based on com-

383 bined lidar, radar reflectivity, and mean doppler velocity measurements, *Journal Of*

384 *Geophysical Research-Atmospheres, 108*.

385 Fridlind, A. M., A. S. Ackerman, E. J. Jensen, A. J. Heymsfield, M. R. Poellot, D. E.

386 Stevens, D. Wang, L. M. Miloshevich, D. Baumgardner, R. P. Lawson, J. C. Wilson,

387 R. C. Flagan, J. H. Seinfeld, H. H. Jonsson, T. M. VanReken, V. Varutbangkul, and

388 T. A. Rissman (2004), Evidence for the predominance of mid-tropospheric aerosols as

389 subtropical anvil nuclei, *Science, 304*, 718–722.

390 Gultepe, I., G. A. Isaac, and K. B. Strawbridge (2001), Variability of cloud microphysical

391 and optical parameters obtained from aircraft and satellite remote sensing measure-

392 ments during race, *International Journal Of Climatology, 21*, 507–+.

393 Jensen, E., D. Starr, and O. B. Toon (2004), Mission investigates tropical cirrus clouds,

394 *Eos Trans. AGU, 84*(5), 50.

395 Li, L. H., G. M. Heymsfield, P. E. Racette, L. Tian, and E. Zenker (2004), A 94-ghz

396 cloud radar system on a nasa high-altitude er-2 aircraft, *Journal Of Atmospheric And*

397 *Oceanic Technology, 21*, 1378–1388.

Liao, L., and K. Sassen (1994), Investigation of relationships between Ka-band radar reflectivity and ice and liquid water contents, *Atmospheric Research, 34*, 231–248.

Liu, C. L., and A. J. Illingworth (2000), Toward more accurate retrievals of ice water content from radar measurements of clouds, *Journal Of Applied Meteorology, 39*, 1130–1146.

Nasiri, S. L., B. A. Baum, A. J. Heymsfield, P. Yang, M. R. Poellot, D. P. Kratz, and Y. X. Hu (2002), The development of midlatitude cirrus models for modis using fire-i, fire-ii, and arm in situ data, *Journal Of Applied Meteorology, 41*, 197–217.

Norris, J. R. (2000), What can cloud observations tell us about climate variability?, *Space Science Reviews, 94*, 375–380.

Pawlowska, H., J. L. Brenguier, Y. Fouquart, W. Armbruster, S. Bakan, J. Descloitres, J. Fischer, C. Flamant, A. Fouilloux, J. F. Gayet, S. Gosh, P. Jonas, F. Parol, J. Pelon, and L. Schuller (2000), Microphysical and radiative properties of stratocumulus clouds: the eucrex mission 206 case study, *Atmospheric Research, 55*, 85–102.

Sassen, K., Z. Wang, V. I. Khvorostyanov, G. L. Stephens, and A. Bennedetti (2002), Cirrus cloud ice water content radar algorithm evaluation using an explicit cloud microphysical model, *Journal Of Applied Meteorology, 41*, 620–628.

Scott, S. G., T. P. Bui, K. R. Chan, and S. W. Bowen (1990), The meteorological measurement system on the NASA ER-2 aircraft, *Journal of Atmospheric and Oceanic Technology, 7*(4), 525–540.

Stephens, G. L. (2005), Cloud feedbacks in the climate system: a critical review, *Journal of Climate, 18*, 237–273.

420 Stephens, G. L., D. G. Vane, R. J. Boain, G. G. Mace, K. Sassen, Z. E. Wang, A. J.

421 Illingworth, E. J. O'Connor, W. B. Rossow, S. L. Durden, S. D. Miller, R. T. Austin,

422 A. Benedetti, and C. Mitrescu (2002), The cloudsat mission and the a-train - a new

423 dimension of space-based observations of clouds and precipitation, *Bulletin Of The*

424 *American Meteorological Society*, *83*, 1771–1790.

425 Stevens, D. E., A. S. Ackerman, and C. S. Bretherton (2002), Effect of domain size

426 and numerical resolution on the simulation of shallow cumulus convection, *Journal Of*

427 *Atmospheric Science*, *59*, 3285–3301.

428 Wang, Z., and K. Sassen (2002a), Cirrus cloud microphysical property retrieval using

429 lidar and radar measurements. part i: Algorithm description and comparison with in

430 situ data, *Journal Of Applied Meteorology*, *41*, 218–229.

431 Wang, Z., and K. Sassen (2002b), Cirrus cloud microphysical property retrieval using

432 lidar and radar measurements. part ii: Midlatitude cirrus microphysical and radiative

433 properties, *Journal Of The Atmospheric Sciences*, *59*, 2291–2302.

434 Weinstock, E. M., J. B. Smith, D. Sayres, J. V. Pittman, N. Allen, and J. G. Anderson

435 (2006a), Measurements of the total water content of cirrus clouds. part ii: Instrument

436 performance and validation, *JOURNAL OF ATMOSPHERIC AND OCEANIC TECH-*

437 *NOLOGY*, *23*(11), 1410–1421.

438 Weinstock, E. M., J. B. Smith, D. Sayres, J. R. Spackman, J. V. Pittman, N. Allen,

439 J. Demusz, M. Greenberg, M. Rivero, L. Solomon, and J. G. Anderson (2006b), Mea-

440 surements of the total water content of cirrus clouds. part i: Instrument details and cal-

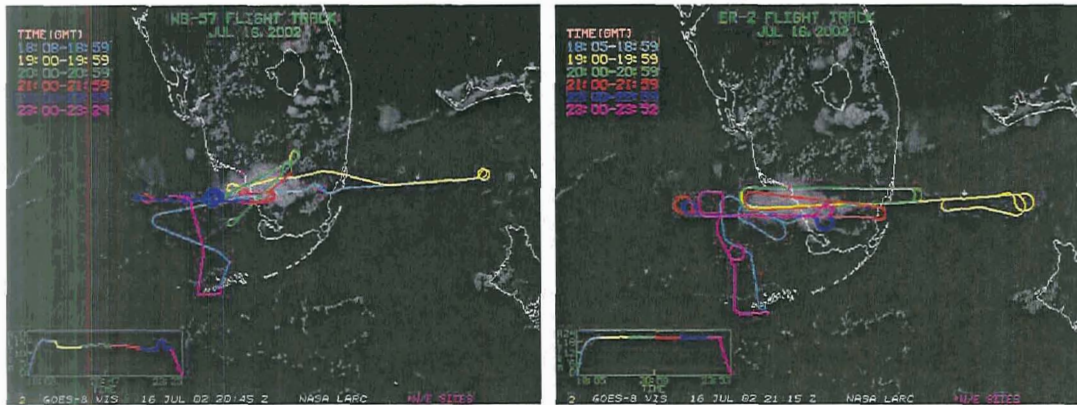441 ibration, *JOURNAL OF ATMOSPHERIC AND OCEANIC TECHNOLOGY*, *23*(11),

442 1397–1409.

Figure 1.   The image on the left shows the flight track of the WB-57 on July 16, 2002 superimposed over a visible GOES image taken at 20:45 UT on July 16th. The flight track is divided into six color coded legs as described by the legend in the image. The image on the right shows the flight track of the ER-2 on July 16, 2002 superimposed over a visible GOES image taken at 21:15 UT on July 16. The legs are divided into approximately the same times periods as with the WB-57. Also shown are the altitudes the aircraft flew at in the lower left hand corner of each image.
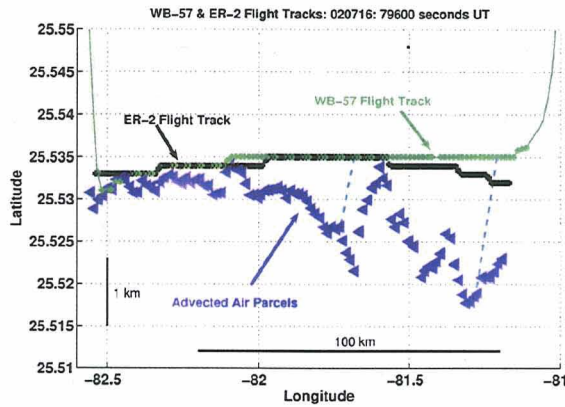
Figure 2.   Advection of air parcels between when the ER-2 and WB-57 sampled the same region. The black points represent the ER-2 flight track, the green points represent the WB-57 flight track and the blue triangles correspond to the air parcels sampled by the WB-57 advected back to where they would have been when the ER-2 sampled this region. The light blue dashed lines show the advection of selected air parcels during the time lag between the ER-2 and WB-57. Note that the x- and y-axes have different scales as indicated by the black scale lines in the figure.
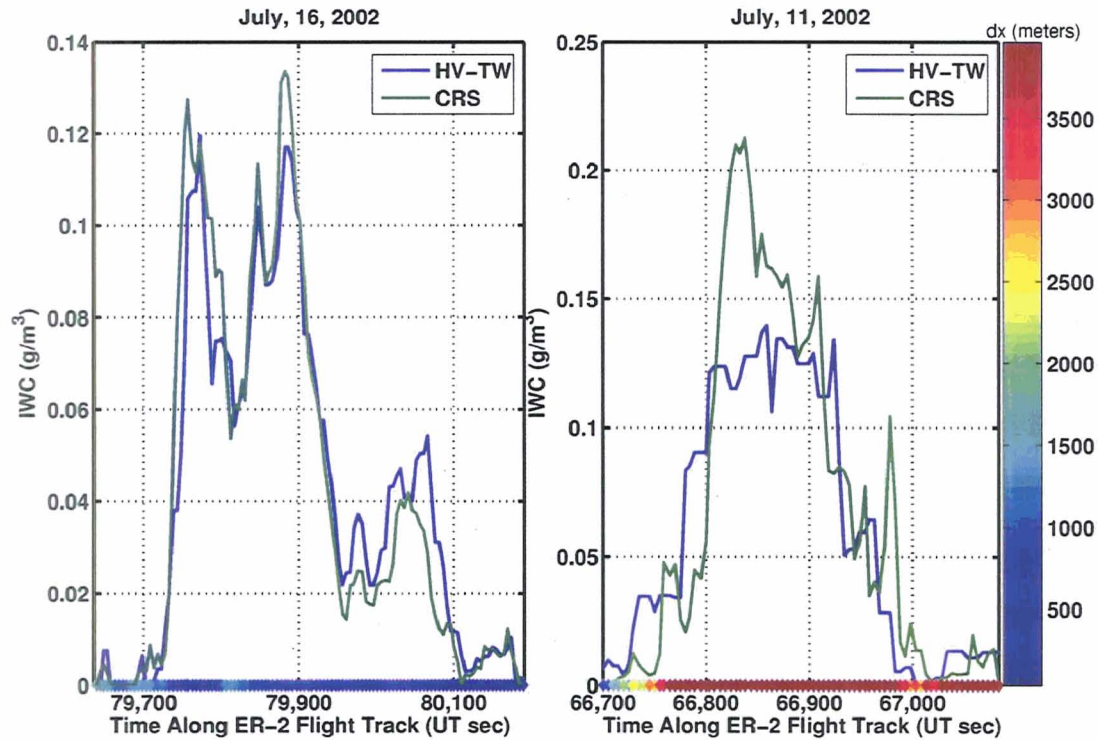
Figure 3.   Comparison of IWC measured *in situ* by the Harvard Total Water instrument and derived from the remote Cloud Radar System, during a cloud transect on July 16th at 79600 seconds UT (left plot) and July 11th at 66700 seconds UT (right plot). HV-TW is plotted in blue and CRS is plotted in green versus time along the ER-2 flight track. The colored points along the bottom of the plots represent the horizontal distance between the air parcels sampled by both instruments. The color code is given by the vertical colorbar to the right of the figures.
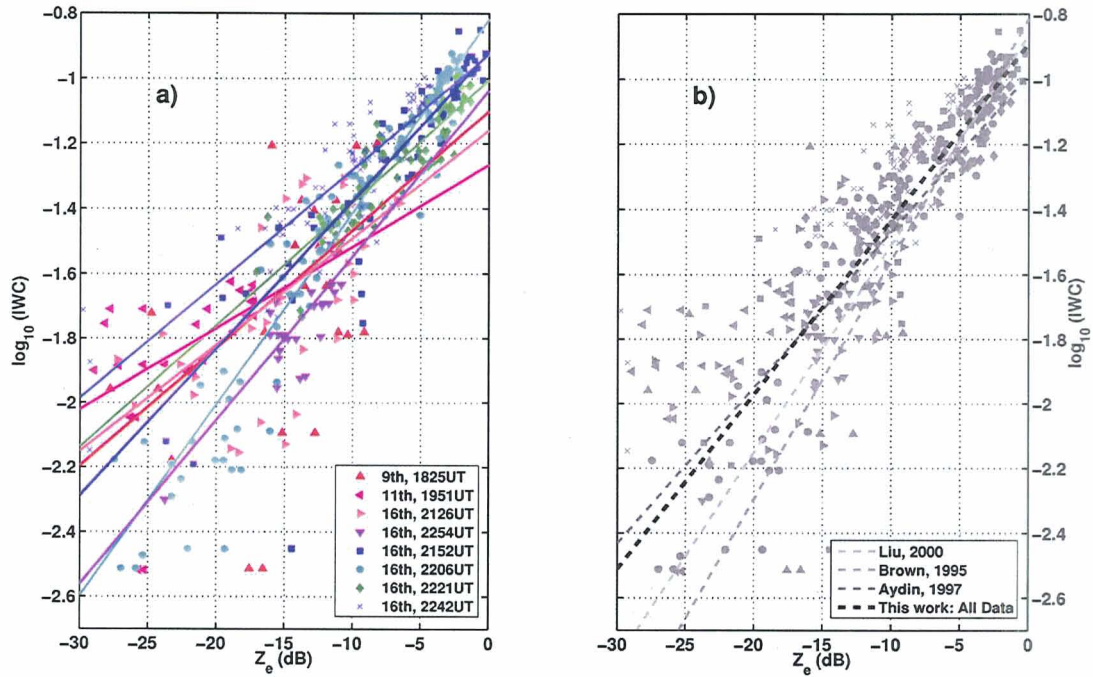
Figure 4. Scatter plots of Z_e (dB) from CRS versus $log_{10}(IWC)$ from HV-TW for 8 different flight segments. Plot a) Each flight segment is plotted in a different color according to the legend in the figure. Colored lines are linear least square fits to the data from each flight segment. Plot b) Plot of all data from the 8 flight segments as well as the least square fit to all the data shown as a thick dark gray dashed line. Also shown are fits using coefficients from Liu [2000], Brown [1995] and Aydin [1997] in the lighter shades of gray.
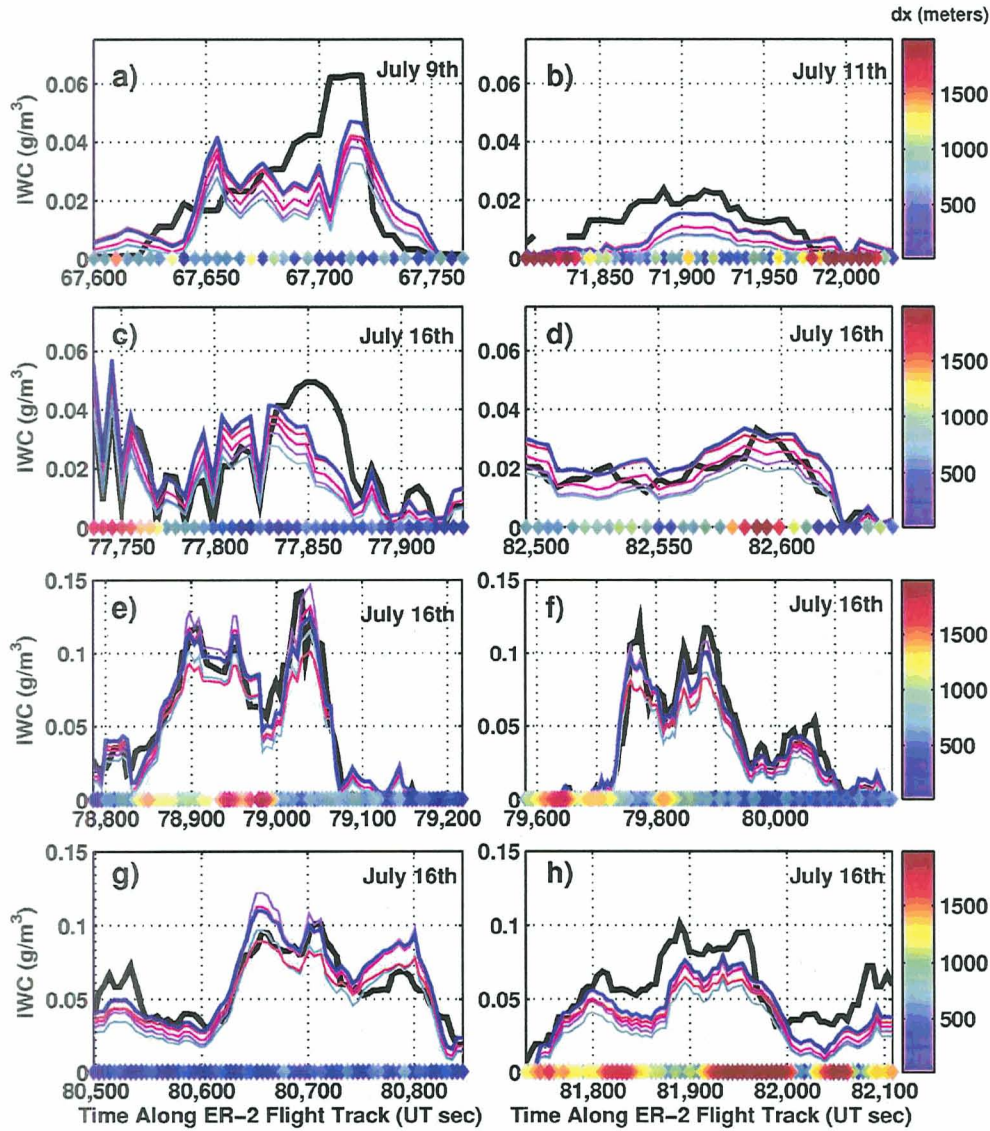
Figure 5.   The 8 plots represent all the comparisons that were made during CRYSTAL-FACE where the air parcels sampled by the WB-57 and ER-2 were within 2 km of each other. For each comparison, the *in situ* IWC data are plotted in black and the derived IWC data using parameters obtained from this work are plotted blue. Also shown are derived IWC data using the relationships described in Brown [1995], Liu [2000], Sassen [1987], and Aydin [1997] in purple, magenta, cyan, and red, respectively.
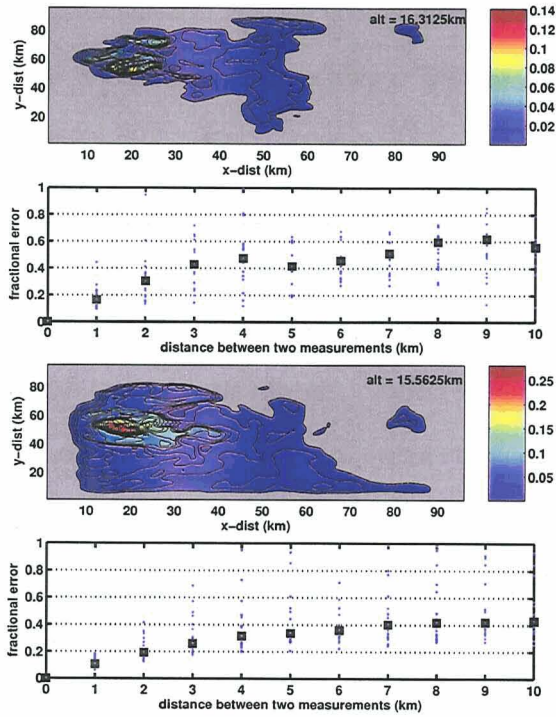
Figure 6. Contour plots show IWC (g/m^3) from the cloud model at altitudes of 16.3 and 15.6 km. The bottom graphs show the fractional error between two measurements of the same cloud as the distance between the measurements increases from 0 to 10 km. The blue points are the average fractional error calculated between two random trajectories through the cloud separated by a distance of 0 to 10 km. The black squares are the median values at each distance for 10 random trajectories.

Table 1.　Parameters for IWC-Z_e relationships from several sources. Coefficients a and b are least squares fits to $IWC = aZ_e^b$ where IWC is measured in g/m^3 and Z_e is measured in $mm^6 m^{-3}$.

Source	Cloud Type	Source of IWC/Z_e	a	b
Sassen, 1987	ground measurements, precipitating ice crystals	size spectra / radar	0.12	0.696
Brown, 1995	N. latitude frontal systems & tropical cirrus	in situ size spectra	0.153	0.74
Liu, 2000	N. latitude frontal systems & tropical cirrus	in situ size spectra	0.137	0.643
Atlas, 1995	midlatitude clouds	in situ size spectra	0.064	0.58
Aydin, 1997	hexagonal columns and plates	modeled size spectra	0.104	0.483
This work	midlatitude anvil cirrus	in situ / radar	0.13	0.54